





Robust functional imaging of taste sensation with a Bessel beam

JISOO HAN,¹ SEONGHOON KIM,^{2,3} PYONGGANG CHOI,^{2,3} SUNGHO LEE,^{2,3} YONGJAE JO,¹  EUNSOO KIM,^{2,3} AND MYUNGHWAN CHOI^{2,3,*} 

¹Department of Biomedical Engineering, Sungkyunkwan University, Suwon 16419, Republic of Korea

²School of Biological Sciences, Seoul National University, Seoul 08826, Republic of Korea

³Institute of Molecular Biology and Genetics, Seoul National University, Seoul 08826, Republic of Korea

*choim@snu.ac.kr

Abstract: Functional imaging of intact taste cells in response to various tastant solutions poses a technical challenge since the refractive index of the immersion medium dynamically changes during tastant delivery. Critically, the focal shift introduced by high-index tastant solutions has been the fundamental limit in experimental design. Here we seek to address this issue by introducing an axially elongated Bessel beam in two-photon microscopy. Compared to the conventional Gaussian beam, the Bessel beam provides superior robustness to the index-induced focal shift, allowing us to acquire near artifact-free imaging of taste cells in response to a physiological taste stimulus.

© 2021 Optical Society of America under the terms of the [OSA Open Access Publishing Agreement](#)

1. Introduction

The initial step in taste sensation is mediated by the orchestrated activity of taste cells on the tongue [1]. Functional imaging of intact taste cells *in vivo* has recently become available due to the development of μ Tongue, a microfluidics-integrated tongue imaging window [2–5]. In μ Tongue, microfluidic channel is interfaced with the dorsal surface of the tongue, providing controlled sensory input to taste cells by switching between artificial saliva and a tastant solution (e.g., an NaCl solution for a salty taste or a sucrose solution for a sweet taste). By introducing intracellular calcium indicators into taste cells, spatiotemporal cellular activities under various tastant stimuli can be recorded in upright two-photon microscopy.

Using the μ Tongue device, the fact that a microfluidic channel (thickness $\approx 300\ \mu\text{m}$) lies between the objective lens and the sample (i.e., taste cells) poses a challenge for microscopic imaging (Fig. 1(a)). Since each tastant solution exhibits a different refractive index (n) which depends on both a solution-specific refractive index (dn/dc) and its concentration (c), the switching of solutions within the channel can introduce dynamic optical aberrations and induce focal shift [6]. This index-induced artifact often overwhelms functional calcium imaging, a technique that typically captures $\sim 10\%$ changes in fluorescence intensity. To ameliorate this issue, we previously introduced the ratiometric approach, which normalizes calcium-sensitive signal (e.g. GCaMP6 in green) by calcium-insensitive signal (e.g. tdTomato in red) [4,5]. This approach helps reduce the artifactual signal, but in practice, it is effective only when the changes in refractive index are small ($\Delta n < 0.003$). Critically, if the focal shift is greater than the imaging depth-of-field, the sequential images are captured at distinct depths over time, a problem that cannot be resolved by post-image-processing [4,7,8]. Consequently, observing the activities of taste cells in response to tastants of high refractive index has been difficult (e.g., $> 200\ \text{mM}$ sucrose or mixture of multiple tastants).

To resolve this technical issue, here, we introduce an axially elongated Bessel beam to a point-scanning two-photon microscope for the μ Tongue-based functional imaging of taste cells (Fig. 1) [9]. In brief, we implemented Bessel beam scanning two-photon microscopy based on a

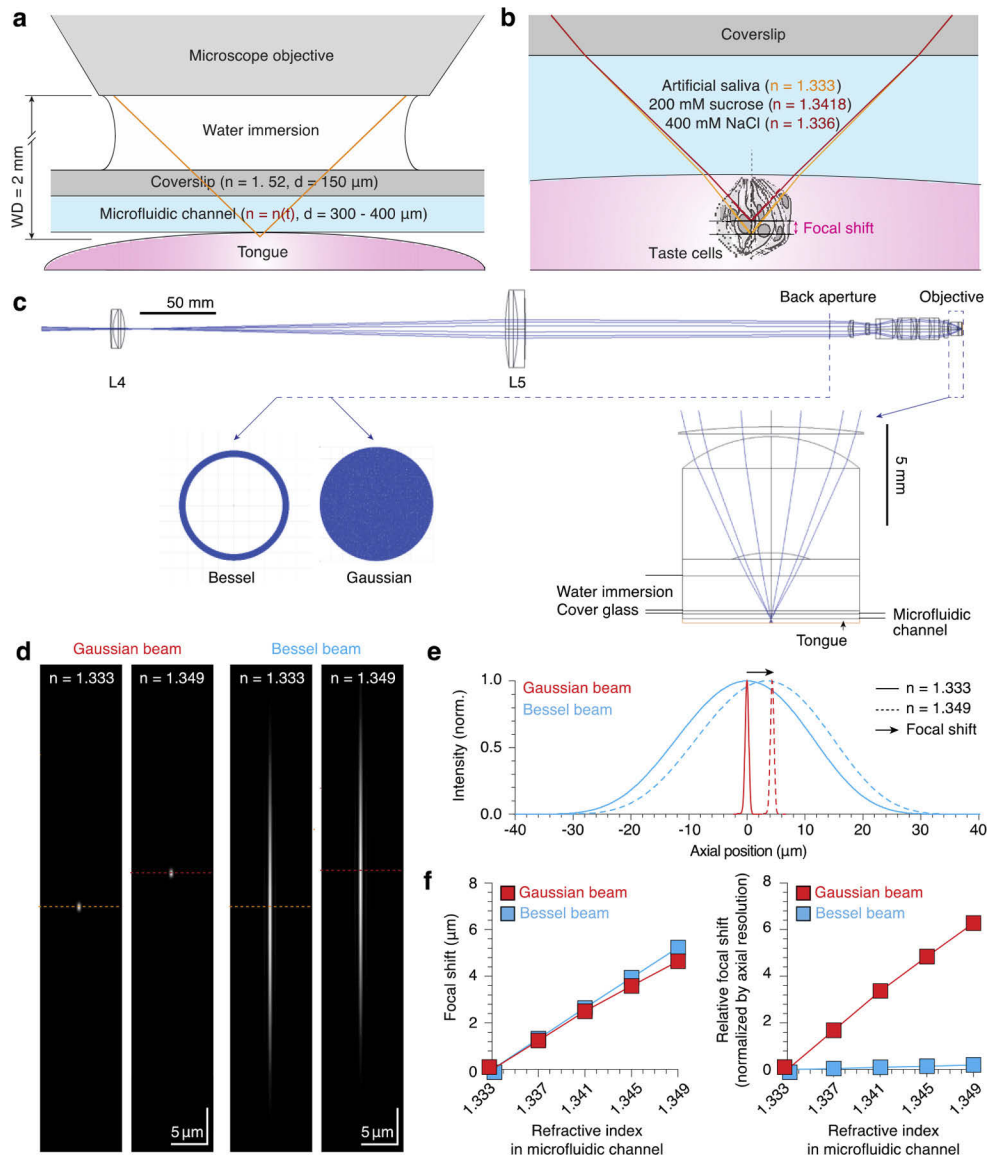


Fig. 1. Refractive index-induced artifacts in μ Tongue. (a) A schematic cross-sectional view of μ Tongue. To reach the target taste cells, the excitation beam passes through water, a cover slip, and the microfluidic channel. The refractive index within the microfluidic channel varies over time according to tastant stimuli. (b) The focal shift introduced by tastant stimuli. (c) A detailed ray diagram used for simulation studies in Zemax. (d) Simulated axial point-spread-functions for the Gaussian and Bessel beams ($\text{NA} = 1$). (e) Axial intensity profiles of the Gaussian and Bessel beams. Axial lengths in FWHM are $0.74 \mu\text{m}$ for the Gaussian beam and $25.9 \mu\text{m}$ for the Bessel beam. (f) Quantification of the focal shift with respect to the refractive index in the microfluidic channel. The relative focal shift was defined as the focal shift normalized by the axial length of the point-spread-function.

spatial-light modulator (SLM) and an annular mask, which provides flexibility in designing a Bessel beam [10,11]. Considering the spherical shape of the taste bud with $\sim 50\ \mu\text{m}$ in diameter and the vertical spindle-shaped taste cells with $\sim 30\ \mu\text{m}$ in length, we designed the Bessel beam to have $\sim 20\ \mu\text{m}$ in length. We quantitatively compared the index-induced artifacts in Gaussian and Bessel beams using a structural similarity index measure (SSIM) and observed that the Bessel beam provided a substantial increase in reliability [12–14]. Last, we demonstrate a proof-of-principle experiment that provides near artifact-free imaging of taste cells in response to a physiological high-indexed tastants, such as high salt or mixture of sweet-salty tastants.

2. Materials and methods

2.1. Fabrication of the annular mask

One side of a quartz wafer (size: $127\ \text{mm} \times 127\ \text{mm}$; thickness: $2.3\ \text{mm}$) was coated with chrome by chemical deposition (thickness: $10\ \mu\text{m}$). A ring-shaped area designed to pass the first-order diffracted light was excluded from the chemical deposition process (detailed design provided in Fig. 2(c); Nepco, South Korea). Then, this chrome-coated wafer was cut to a circular shape with a diameter of $12.7\ \text{mm}$ and was mounted on a $12.7\ \text{mm}$ lens tube (T. Friends, South Korea). A $1 \times 1\ \text{mm}$ tinfoil piece was glued to the center of the annular mask using an optical adhesive (NOA81, Norland Products) to protect the mask from zero-order diffracted light.

2.2. Preparation of bead samples

To measure the lateral and axial resolution, fluorescent microbead samples were prepared as described previously [15]. In brief, an immersion medium was prepared by mixing polydimethylsiloxane (PDMS; Sylgard 184, Sigma-Aldrich) and a curing agent at 10% w/w. Fluorescent beads ($0.1\ \mu\text{m}$; 580/605; F8801, Thermo Fisher Scientific) were added to the PDMS solution and dispersed by vortexing. The mixture was set aside in a vacuum chamber for 1 h to remove air bubbles and then incubated for 2 hours at 60°C until solidified.

2.3. Animal and preparation of *in vivo* experiment

A five-month-old male GAD65-GCaMP6f-tdTomato mouse was used for the *in vivo* experiment [16]. This mouse was obtained by crossbreeding GAD65-Cre mice (#010802, Jackson Laboratory) with CAG-floxed-GCaMP6f-tdTomato mice (#031968, Jackson Laboratory). A detailed procedure of the *in vivo* experiment was described previously [4]. In brief, the mouse was anesthetized with a mixture of $0.12\ \text{mg/g}$ ketamine (Yuhan Corp.) and $0.01\ \text{mg/g}$ xylazine (Bayer Korea) intraperitoneally. To minimize movement artifacts, the mouse skull was fixed to a head post after removing the scalp and periosteum. Subsequently, the mouse tongue was gently withdrawn and attached to the bottom piece of the μTongue device. Last, the upper piece of the μTongue device was placed on top of the tongue. All animal experiments were performed in compliance with institutional guidelines and were approved by the respective subcommittees for research animal care at Sungkyunkwan University and Seoul National University.

2.4. Two-photon optical path and *in vivo* imaging

A femtosecond fiber laser (wavelength: $920\ \text{nm}$, repetition rate: $80\ \text{MHz}$, output power: $1.2\ \text{W}$, pulse width: $100\ \text{fs}$; FemtoFiber ultra 920, Toptica Photonics) was used as an excitation source for the customized upright two-photon microscope (Bergamo II, Thorlabs). The excitation beam was expanded to $4\ \text{mm}$ in diameter ($1/e^2$) and then was split into Gaussian and Bessel paths by a halfwave plate and a polarizing beam splitter. For the Gaussian path, the beam was relayed to a dual-axis galvo-scanner (OPX1210, Thorlabs), which was 4f-conjugated to the back pupil plane of the water-immersion objective lens ($25\times$, $1.1\ \text{NA}$; Nikon). For Bessel imaging, the beam was relayed to a reflective SLM (ODPDM512-1064, Meadowlark) with a periodic ring pattern. Then,

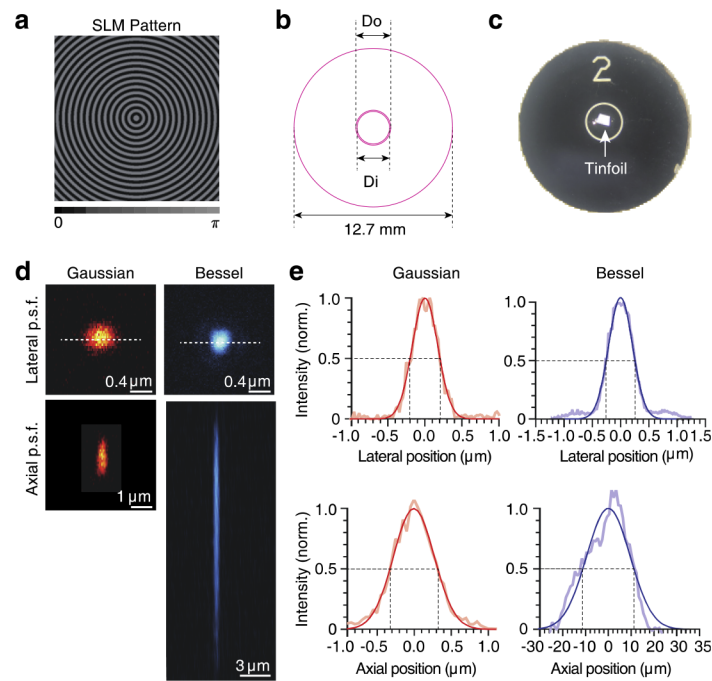


Fig. 2. The fabrication of an annular mask and the optical characterization. (a) The input pattern for the SLM. The binary concentric ring image has an alternating phase delay of 0 and π with a grating period of 18.41 pixels. (b,c) The annular mask. The diameter of an annular mask is 12.7 mm and was designed to fit into a half-inch optical mount. The filter size of inner diameter (D_i) is 2.536 mm, and the outer diameter (D_o) is 2.80 mm. A small piece of tin foil (~ 1 mm in size) was glued to the center to avoid damage by the first-order diffraction beam. (d) Point-spread-functions (p.s.f.) for the Gaussian and Bessel beams. A 100 nm fluorescence bead was used as a sample. (e) The intensity profiles for the Gaussian and Bessel paths. The data are fitted to a Gaussian function. Dot lines indicate where the FWHM is quantified. Axial resolutions for Gaussian and Bessel beams were ~ 1.3 μm and ~ 22.5 μm , respectively.

the diffracted beam was filtered by the pre-designed annular aperture, which was conjugated to the galvanomirrors and back focal plane of the objective lens. The laser powers at the sample were 8–15 mW for the Gaussian path and 40 mW for the Bessel path. Emitted light was collected by two GaAsP PMTs for ratiometric calcium recording (520/50 nm for GCaMP6 and 607/70 nm for tdTomato) via the non-descanned path.

2.5. Image processing and data analysis

Image processing and design of the annular ring was performed using ImageJ (National Institutes of Health) and MATLAB (Mathwork), respectively. Optic simulation of the index-induced focal shifts was performed using OpticStudio (Zemax). Statistical analysis and data regression was performed using GraphPad Prism.

3. Results

3.1. Rationale

To image the taste cells using the μTongue device, the excitation beam from the water-immersion objective lens passes through multiple layers. These layers are composed of immersion media

($n = 1.333$, $d \approx 1.5$ mm), a coverslip ($n = 1.52$, $d \approx 0.15$ mm), and a microfluidic channel filled with either artificial saliva ($n = 1.333$, $d \approx 0.3$ mm) or a tastant solution ($n > 1.333$, $d \approx 0.3$ mm) (Fig. 1(a),(b)). To evoke the functional activity of taste cells, the fluid within the microfluidic channel is changed from artificial saliva to a tastant solution, typically for a period of 5–20 s, after which the solution returns to artificial saliva. Consequently, the taste stimuli inevitably accompany a change in refractive index of the immersion media and results in induced optical aberrations including axial shifts in the image plane.

To quantitatively investigate the influence of physiological tastant solutions in microscopic imaging, first, we measured the refractive indices of various physiological tastant solutions covering the five basic tastants – sweet, umami, bitter, sour, and salty – using a digital refractometer. Consistent with the previous report [6], the refractive indices of the solutions increased proportionally with tastant concentration (e.g. dn/dc : 9.3 mM^{-1} for NaCl and 47.8 mM^{-1} for sucrose; Table 1). Next, we performed optical simulations using the refractive indices of the tastant solutions and quantified the degree of focal shift (Fig. 1(c)-(f)). In our optical simulation using a conventional Gaussian beam, the change in refractive index within the channel resulted in upward focal shifts of $\sim 0.3 \text{ }\mu\text{m}$ for each Δn of 0.001. Notably, a physiological sweet-tasting solution of 200 mM sucrose ($n = 1.3418$) introduces a $\sim 2.5 \text{ }\mu\text{m}$ focal shift (Fig. 1(d)), which is comparable to the diffraction-limited depth-of-field ($\sim 1 \text{ }\mu\text{m}$ at $NA = 1$). Then, a time-series readout would sample at distinct depths over time. Consequently, the applications of μTongue have been restricted to tastant solutions with low refractive indices.

Table 1. Refractive indices of physiologic tastant solutions^a

Tastant	Concentration (c)	Refractive index (n)	dn/dc (10^{-3} M^{-1})
Artificial saliva	-	1.333	-
Quinine	5 mM	1.334	93.27
Ace K (acesulfame K)	40 mM	1.334	24.03
Sucrose	200 mM	1.343	47.83
Citric acid	10 mM	1.333	23.49
NaCl	400 mM	1.336	9.30
MPG (monopotassium glutamate)	100 mM	1.336	24.66

^aModified from bioRxiv, 371682 (2018).

We reasoned that because the Bessel beam exhibits an axially elongated point-spread-function (i.e., depth-of-field), even when under the influence of index-induced focal shifts, the time-series readout would sample mostly in the originally targeted location. Considering the typical axial length of murine taste cells (20–30 μm), we designed the Bessel beam to have an axial resolution of $\sim 20 \text{ }\mu\text{m}$ for the simulation studies. Indeed, although the degree of the focal shift was similar with a Bessel beam compared to a Gaussian beam, the focal shifts relative to the depth-of-field (i.e., proportion of index-induced artifact) were over one order-of-magnitude lower than the Gaussian beam.

3.2. Design and implementation of Bessel beam scanning microscopy

To experimentally test the concept, we designed a upright laser-scanning two-photon microscope that incorporated both Gaussian and Bessel beam paths (Fig. S1) [9]. A 920 nm fiber femtosecond laser was split into Gaussian and Bessel paths, and then, it was coupled to a galvanomirror-based two-photon system. To generate the Bessel beam, the Gaussian beam was phase modulated by a spatial-light modulator (SLM) with a biphasic concentric ring pattern, and the first-order

diffracted beam was filtered by an annular aperture at the Fourier plane of the SLM. The annular mask was $4f$ conjugated to the galvanomirrors and the objective back aperture to generate a Bessel beam at the sample.

Considering the size and shape of a typical murine fungiform taste bud, we set the target axial length for the Bessel beam to $\sim 20\ \mu\text{m}$ in full-width-half-maximum (FWHM). To generate optimal ring illumination at the back aperture, we performed a numerical simulation of electric field distribution at the mask plane using open source MATLAB code provided by the Na Ji group [10]. After inputting the design parameters of our system (input beam diameter = 4 mm, objective magnification = $25\times$, focal lengths for relay lenses), we obtained the optimal design for the annular aperture (inner diameter = 2.530 mm, outer diameter = 2.80 mm) and the binary phase pattern at the SLM (period = 18.41 pixels; Fig. 2(a)). These parameters yielded a Bessel beam of $21\ \mu\text{m}$ with an effective NA of 0.7 (Fig. S1). The annular aperture was fabricated as designed from patterned coating of chrome in a silicon wafer with a tinfoil piece attached at the center to minimize damage caused by the zeroth-order beam (Fig. 2(b),(c)).

Using 100 nm fluorescent beads, we measured the resolutions of the Gaussian and Bessel path (refer to the Materials and Methods section for a detailed explanation of sample preparation). A fluorescent bead was imaged at a lateral sampling rate of 20 nm/pixel and axial sampling steps of $0.1\ \mu\text{m}$ and $1\ \mu\text{m}$ for the Gaussian and Bessel beams, respectively. The laser powers at the sample were set to 1–2 mW for the Gaussian beam and 10 mW for the Bessel beam. The measured point-spread-functions were fitted to a Gaussian function. The lateral resolutions were $\sim 400\ \text{nm}$ for both the Gaussian and Bessel paths, and the axial resolution was $\sim 1.3\ \mu\text{m}$ for the Gaussian path and $\sim 22.5\ \mu\text{m}$ for the Bessel path. These measurements were in good agreement with our optical simulation (Fig. 2) [10].

3.3. Applications in functional imaging *in vivo*

We performed a proof-of-principle experiment to test whether the Bessel beam is resilient to index-induced artifacts in μTongue -based imaging on taste cells *in vivo*. We used a transgenic mouse line that expresses both calcium-sensitive and calcium-insensitive indicators in taste cells (GAD65-GCaMP6-tdTomato). As expected by their point-spread-functions, a single-slice image acquired by the Bessel beam was comparable to the corresponding z-projected Gaussian image (Fig. 3(a)). We investigated the influence of tastant delivery on imaging stability (Fig. 3(b),(c)). For this study, we analyzed only the calcium-insensitive signal (i.e., tdTomato in a red channel), since its temporal fluctuation reflects tastant-induced artifacts. While performing time-series imaging of a taste bud with either Gaussian or Bessel beams, we switched the solutions in a microfluidic channel from artificial saliva to sucrose solutions ranging from 0 to 400 mM ($n = 1.333\text{--}1.352$) for a period of 20 s. Consistent with our simulation, we observed dramatic time-varying focal shifts with the Gaussian beam in response to the sucrose solutions in dose-dependent manner, whereas minimal change was noted by the Bessel beam (Fig. 3(b),(c)). To quantify the index-induced imaging artifact over time, we used SSIM, which has been widely used for estimating pixel-based image distortion [12–14]. The change in SSIM index, representing the magnitude of the imaging artifact, was quantified for the taste bud image. Compared to the Gaussian beam, the Bessel beam resulted in ~ 5 -folds improvement in robustness to index-induced artifacts (Fig. 3(d),(e)).

Lastly, we applied our approach to study functional activities of taste cells in response to high-indexed tastant solutions. We used sweet-salty mixtures composed of 400 mM NaCl and up to 200 mM sucrose, since they are expected to generate reliable functional responses on the taste cells in our mouse model (GAD65-GCaMP6-tdTomato) and also introduce severe index-induced artifact ($n = 1.336\text{--}1.344$). While performing time-series imaging of the taste cells with either Gaussian or Bessel beams, taste cells were exposed to the tastant mixtures for a period of 20 s (Fig. 4). In the taste bud we examined, a subpopulation of taste cells showed

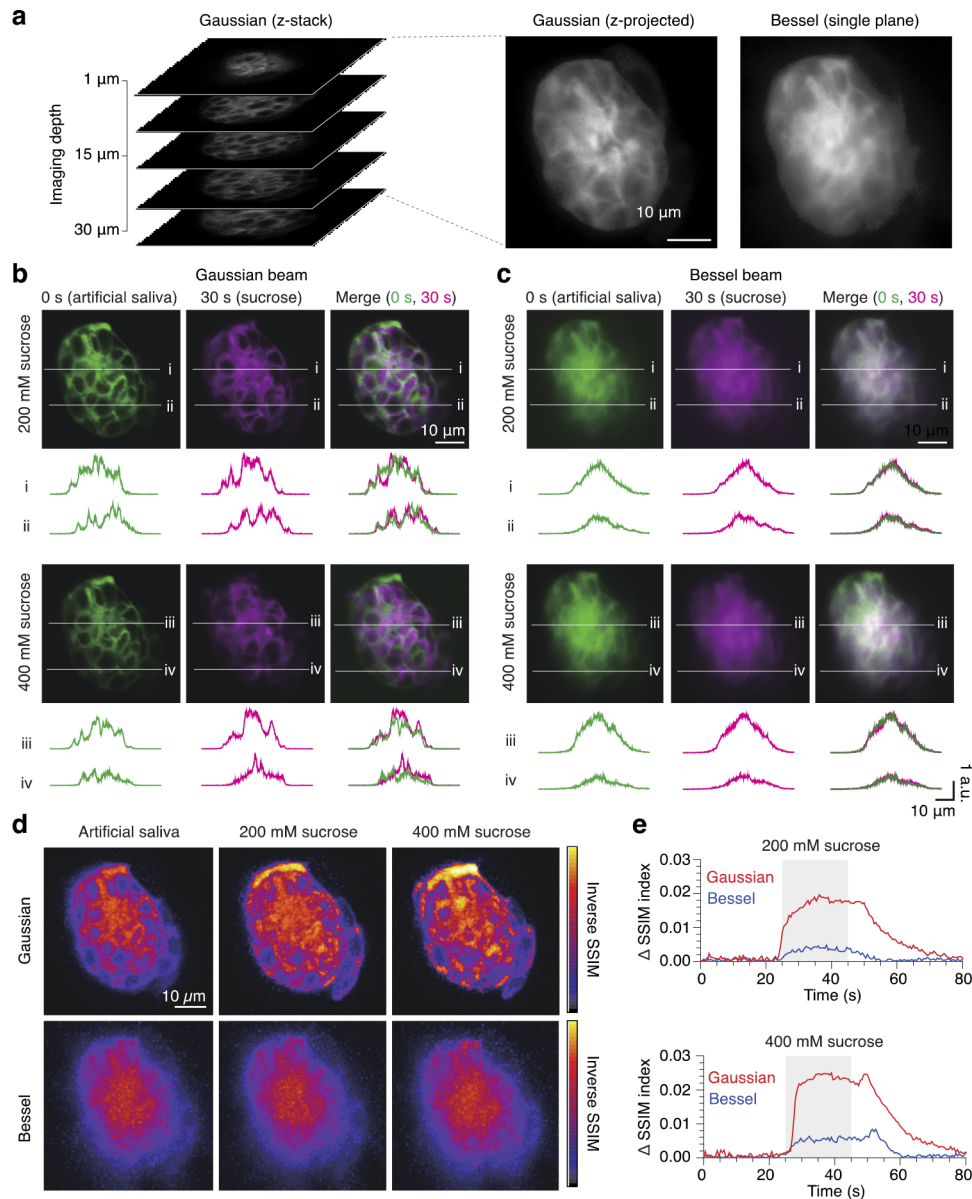


Fig. 3. Comparison of tastant-induced artifacts in Gaussian and Bessel beams. To access the index-induced artifact, only the calcium-insensitive tdTomato signal is investigated in a GAD65-GCaMP6-tdTomato mouse. (a) A representative fluorescent image of a taste bud taken with the Gaussian and Bessel beams. Note that the z-projected Gaussian image is comparable to the single plane Bessel image. (b,c) Representative index-induced artifacts in response to 200 mM and 400 mM sucrose. The Gaussian images (b) exhibit noticeable change in structure, whereas the Bessel images (c) are relatively stable. Line intensity profiles (i-iv) are shown below. a.u., arbitrary unit. (d) SSIM maps before and after the tastant delivery. The pseudo-colored maps indicate the inversed SSIM value, corresponding to the degree of index-induced structural change. (e) Dynamics of the index-induced structural change. The graphs represent the change in SSIM values over time acquired in (d). The shaded areas indicate the duration of the tastant delivery (200 mM and 400 mM sucrose).

increased intracellular calcium signal in sync with high salt stimulus, and sucrose-responsive cells were not observed [17,18]. Although sucrose did not evoke further functional responses in this taste bud, the index-induced artifact severely interfered the recording of both GCaMP6 and tdTomato channels. The ratiometric analysis helped ameliorating the index-induced artifact in both Gaussian and Bessel imaging, but notably, the Gaussian imaging failed to reliably capture the salty-responsive cell (cell 1 in Fig. 4(b)) when 200 mM sucrose was added [4,7,8]. By contrast, Bessel beam showed robustness to the index-induced artifact so that the salty-responsive cell was reliably identified even with influence of high-indexed sucrose solution.

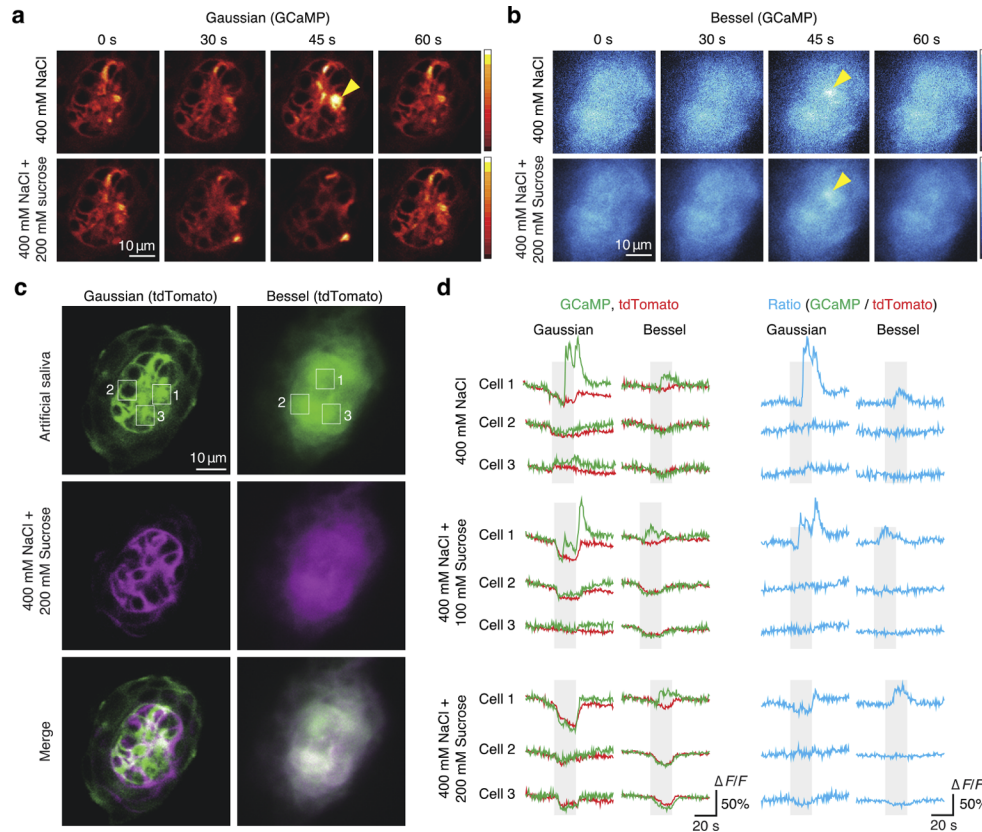


Fig. 4. Demonstration of the robust functional imaging of taste cells with the Bessel beam. (a, b) Time-series GCaMP-based calcium images of a taste bud in response to salty (400 mM NaCl) and salty-sweet (400 mM NaCl + 200 mM sucrose) tastants acquired by the Gaussian (a) and Bessel (b) mode. Tastants were exposed to the taste bud for ~20 s (25–45 s). The yellow arrowheads indicate the taste cells exhibiting the apparent increase in intracellular calcium. (c) Representative Gaussian and Bessel images of a taste bud acquired before (artificial saliva) and after the tastant delivery (400 mM NaCl + 200 mM sucrose). The signal represents tdTomato fluorescence. Note in the merged view that Bessel images are highly stable even with influence of the high-indexed tastant. (d) Representative intensity traces of GCaMP, tdTomato and their ratio (GCaMP divided by tdTomato) acquired with multiple tastant stimuli: 400 mM NaCl (top), 400 mM NaCl with 100 mM sucrose (middle), 400 mM NaCl with 200 mM sucrose (bottom). The salty-responsive signal observed in Cell 1 was reliably acquired by the Bessel beam even with high-index induced artifacts (e.g. 400 mM NaCl with 100 mM or 200 mM sucrose). The shaded areas indicate the duration of tastant stimuli

4. Conclusion and discussion

We report that an axially elongated Bessel beam can effectively reduce index-induced artifacts, which are an inevitable problem during functional imaging of taste cells *in vivo*. This approach will provide a more reliable method to measure the functional activities of taste cells exposed to high concentrations of tastants, especially those that are difficult to study with a conventional Gaussian beam.

Although we mainly focused on the focal shift, other dynamic aberrations also occur especially during the switching of tastant solutions. Moreover, motion artifacts caused by breathing and heart beating is inevitable *in vivo*. Consequently, ratiometric approach was necessary for reliable readout of functional cellular activities even with Bessel beams (as illustrated in Fig. 4(d)) [4]. Self-healing properties of Bessel beam may help reducing the other aberrations, but it remains to be investigated [9].

Due to the vertical spindle-shaped morphology of taste cells and spatial sparsity of taste-responsive cells, the reduced axial resolution of Bessel beam did not complicate identification of functional cellular activity (Fig. 4). However, the low axial resolution of Bessel beam may be disadvantageous if distinct sources of signals overlap axially. This problem may be mitigated by applying post-image processing tools, such as source separation by non-negative matrix factorization [19], which demonstrated to be effective in simultaneous functional recording of multiple superimposed neurons [20–22]. Alternatively, the Gaussian beam with high axial resolution can be used with online compensation of focal drift using remote focusing [23,24].

Funding. Seoul National University (New Faculty Startup Fund); Samsung Science and Technology Foundation (SSTF-BA2002-14).

Author Contributions. M.C. conceived and supervised the study. J.H. performed the experiments and data analysis. S.K. performed the optical simulation. S.L. and P.C. assisted the experiments. Y.J. and E.K. fabricated the annular masks. M.C. and J.H. cowrote the manuscript with input from all authors.

Disclosures. The authors declare no conflicts of interest.

Data availability. Data underlying the results presented in this paper are not publicly available at this time but may be obtained from the authors upon reasonable request.

Supplemental document. See [Supplement 1](#) for supporting content.

References

1. S. D. Roper and N. Chaudhari, "Taste buds: cells, signals and synapses," *Nat. Rev. Neurosci.* **18**(8), 485–497 (2017).
2. M. Choi, S. J. J. Kwok, and S. H. Yun, "In vivo fluorescence microscopy: lessons from observing cell behavior in their native environment," *Physiology* **30**(1), 40–49 (2015).
3. M. Choi, W. M. Lee, and S. H. Yun, "Intravital microscopic interrogation of peripheral taste sensation," *Sci. Rep.* **5**(1), 8661 (2015).
4. J. Han and M. Choi, "Comprehensive functional screening of taste sensation in vivo," *bioRxiv* **16419**, 371682 (2018).
5. J. Han, P. Choi, and M. Choi, "µTongue : a microfluidics-based functional imaging platform for the tongue in vivo," *JoVE* **1**(170), e62361 (2021).
6. F. A. Glover and J. D. S. Goulden, "Relationship between refractive index and concentration of solutions," *Nature* **200**(4912), 1165–1166 (1963).
7. T. Thestrup, J. Litzlbauer, I. Bartholomäus, M. Mues, L. Russo, H. Dana, Y. Kovalchuk, Y. Liang, G. Kalamakis, Y. Laukat, S. Becker, G. Witte, A. Geiger, T. Allen, L. C. Rome, T. W. Chen, D. S. Kim, O. Garaschuk, C. Griesinger, and O. Griesbeck, "Optimized ratiometric calcium sensors for functional in vivo imaging of neurons and T lymphocytes," *Nat. Methods* **11**(2), 175–182 (2014).
8. J. P. Nguyen, F. B. Shipley, A. N. Linder, G. S. Plummer, J. W. Shaevitz, and A. M. Leifer, "Whole-brain calcium imaging with cellular resolution in freely behaving *C. elegans*," *Proc. Natl. Acad. Sci.* **113**(8), E1074–E1081 (2016).
9. G. Thériault, M. Cottet, A. Castonguay, and N. McCarthy, "Extended two-photon microscopy in live samples with Bessel beams : steadier focus, faster volume scans, and simpler stereoscopic imaging," *Front. Cell. Neurosci.* **8**(139), 1–11 (2014).
10. R. Lu, W. Sun, Y. Liang, A. Kerlin, J. Bierfeld, J. D. Seelig, D. E. Wilson, B. Scholl, B. Mohar, M. Tanimoto, M. Koyama, D. Fitzpatrick, M. B. Orger, and N. Ji, "Video-rate volumetric functional imaging of the brain at synaptic resolution," *Nat. Neurosci.* **20**(4), 620–628 (2017).
11. J. L. Fan, J. A. Rivera, W. Sun, J. Peterson, H. Haeberle, S. Rubin, and N. Ji, "High-speed volumetric two-photon fluorescence imaging of neurovascular dynamics," *Nat. Commun.* **11**(1), 6020 (2020).

12. Z. Wang and A. C. Bovik, "A universal image quality index," *IEEE Signal Process. Lett.* **9**(3), 81–84 (2002).
13. Z. Wang, A. C. Bovik, H. R. Sheikh, and E. P. Simoncelli, "Image quality assessment: From error visibility to structural similarity," *IEEE Trans. on Image Process.* **13**(4), 600–612 (2004).
14. K. Gu, S. Wang, G. Zhai, W. Lin, X. Yang, and W. Zhang, "Analysis of distortion distribution for pooling in image quality prediction," *IEEE Trans. Broadcast.* **62**(2), 446–456 (2016).
15. J. Han, S. Lee, P. Choi, J. Wu, K. Lee, Q. Dai, J. Park, K.-B. Lee, and M. Choi, "Improving collection efficiency in two-photon endoscopy with reflective waveguiding," *Opt. Express* **26**(25), 32365 (2018).
16. J. K. Roebber, S. D. Roper, and N. Chaudhari, "The role of the anion in salt (NaCl) detection by mouse taste buds," *J. Neurosci.* **39**(32), 6224 (2019).
17. A. Vandenbeuch, T. R. Clapp, and S. C. Kinnamon, "Amiloride-sensitive channels in type I fungiform taste cells in mouse," *BMC Neurosci.* **9**(1), 1–13 (2008).
18. N. Chaudhari and S. D. Roper, "The cell biology of taste," *J. Cell Biol.* **190**(3), 285–296 (2010).
19. W. Yang, J.-E. Kang Miller, L. Carrillo-Reid, E. Pnevmatikakis, L. Paninski, R. Yuste, and D. S. Peterka, "Simultaneous Multi-plane Imaging of Neural Circuits," *Neuron* **89**(2), 269–284 (2016).
20. D. D. Lee and H. Sebastian Seung, "Learning the parts of objects by non-negative matrix factorization," *Nature* **401**(6755), 788–791 (1999).
21. A. S. Montcuquet, L. Hervé, F. Navarro, J. M. Dinten, and J. I. Mars, "In vivo fluorescence spectra unmixing and autofluorescence removal by sparse nonnegative matrix factorization," *IEEE Trans. Biomed. Eng.* **58**(9), 2554–2565 (2011).
22. T. Pengo, A. Muñoz-Barrutia, I. Zudaire, and C. Ortiz-de-Solorzano, "Efficient blind spectral unmixing of fluorescently labeled samples using multi-layer non-negative matrix factorization," *PLoS ONE* **8**(11), e78504 (2013).
23. E. J. Botcherby, R. Juškaitis, M. J. Booth, and T. Wilson, "An optical technique for remote focusing in microscopy," *Opt. Commun.* **281**(4), 880–887 (2008).
24. Y. Yang, W. Chen, J. L. Fan, and N. Ji, "Adaptive optics enables aberration-free single-objective remote focusing for two-photon fluorescence microscopy," *Biomed. Opt. Express* **12**(1), 354 (2021).